3FGL J1924.8-1034: A spatially extended stable unidentified GeV source?

Zi-Qing Xia,[1,2] Kai-Kai Duan,[1,3] Shang Li,[1,3,*] Yun-Feng Liang,[1,3,†] Zhao-Qiang Shen,[1,3,‡] Chuan Yue,[1,3]
Yuan-Peng Wang,[1,3] Qiang Yuan,[1,2] Yi-Zhong Fan,[1,2,§] Jian Wu,[1,2] and Jin Chang[1,2]

[1]Key Laboratory of Dark Matter and Space Astronomy, Purple Mountain Observatory,
Chinese Academy of Sciences, Nanjing 210008, China
[2]School of Astronomy and Space Science, University of Science and Technology of China,
Hefei, Anhui 230026, China
[3]University of Chinese Academy of Sciences, Beijing 100012, China
(Received 17 November 2016; published 19 May 2017)

Milky Way–like galaxies are predicted to host a very large number of dark matter subhalos. Some massive and nearby subhalos could generate detectable gamma rays, appearing as unidentified, spatially extended and stable gamma-ray sources. We search for such sources in the third Fermi Large Area Telescope source list (3FGL) and report the identification of a new candidate, 3FGL J1924.8-1034. With the Fermi-LAT Pass 8 data, we find that 3FGL J1924.8-1034 is spatially extended at a high confidence level of 5.4σ, with a best-fit extension radius of $\sim$0.15°. No significant variability has been found and its gamma-ray spectrum is well fitted by the dark matter annihilation into $b\bar{b}$ with a mass of $\sim$43 GeV. All these facts make 3FGL J1924.8-1034 a possible dark matter subhalo candidate. However, due to the limited angular resolution, the possibility of that the spatial extension of 3FGL J1924.8-1034 is caused by the contamination from the other unresolved point source cannot be ruled out.

I. INTRODUCTION

The total mass-energy of the Universe cannot be explained by the ordinary matter in the standard model of cosmology. Dark matter (DM), an invisible form of matter, is believed to make up a quarter of the energy density of the current Universe. However, nobody knows what it is. Various hypothetical particles have been proposed. As the most widely accepted hypothesis, it is composed of weakly interacting massive particles, which only interact through gravitational and weak forces and may be able to annihilate with each other (or alternatively decay) into stable high-energy particle pairs, including gamma rays, charged particles and neutrinos [1–5]. The identification of these annihilation or decay products is the main goal of dark matter indirect detection experiments.

Among various indirect search methods, observations of the gamma-ray sky have attracted wide attention over the years thanks to the successful and productive performance of the Fermi Large Area Telescope (LAT) [6,7]. Intense dedicated researches have been carried out to catch the gamma-ray radiation from dark matter annihilation or decay utilizing the Fermi-LAT data towards many different observational targets, such as the dwarf spherical galaxies [8–16], galaxy clusters [17–21], the Galactic center [22–28], and the extragalactic gamma-ray background [29–31]. Among these various targets, the most promising are the Galactic center for its high density of dark matter and the dwarf spherical galaxies (dSphs) for the low astrophysical gamma-ray backgrounds. However so far no reliable dark matter signal has been identified [6]. The joint analysis of 15 dwarf spheroidal galaxies sets the most stringent constraint on the cross section of DM annihilating through $b\bar{b}$ and $\tau^+\tau^-$ channels [10].

In this work, we focus on dark matter subhalos. N-body simulations reveal that dark matter structures form hierarchically, i.e., the dark matter gathers together to form small halos, and then small halos merge repeatedly to create ever larger systems [32]. As a consequence of this process, a Milky Way–like galaxy is predicted to host tens of thousands of galactic DM subhalos [33,34]. The most massive of these subhalos are expected to host the known dSphs, while some small subhalos may completely lack any astrophysical counterparts for no significant quantity of baryonic matter. However, some of these small subhalos, if still massive enough and close enough to the Earth, may generate detectable gamma rays, observed as a group of unidentified gamma-ray sources. For example, assuming a dark matter particle mass of $\sim$100 GeV and an annihilation cross section of $\langle\sigma v\rangle \simeq 2\times 10^{-26}\,\mathrm{cm^3\,s^{-1}}$, Fermi-LAT might have recorded $\sim$10 dark matter subhalos [35–40]. To further distinguish between the unidentified astrophysical sources and the dark matter subhalos, the spatial extension likely plays an important role since a spatially extended stable source without any

*Corresponding author.
lishang@pmo.ac.cn
†Corresponding author.
liangyf@pmo.ac.cn
‡Corresponding author.
zqshen@pmo.ac.cn
§Corresponding author.
yzfan@pmo.ac.cn

association in other wavelengths is hard to explain in astrophysical scenarios [41]. Consequently, we consider the unidentified stable gamma-ray sources with extendible structure at a confidence level of $> 5\sigma$ ($\Delta TS_{ext} > 25$) as DM subhalo candidates.

The rest of this paper is structured as follows. In the second section, we present our selection of DM subhalo candidates and the comparison with the previous literature. In the third section, we describe details of the Fermi data analysis focusing on our single DM subhalo candidate. Finally, in the fourth section, we summarize our results and discuss some uncertainties in our work.

II. THE SELECTION OF DM SUBHALO CANDIDATES

There are 3033 sources included in the third Fermi Large Area Telescope source list (3FGL) [42]. 992 of them have not been identified in other wavelengths. In our investigation, we searched for dark matter subhalo candidates among the unidentified stable (with Variability_Index less than 80) sources at galactic latitudes $|b| > 10°$ without any cut in gamma-ray flux intensity in the 3FGL. The spatial characteristics of all these sources are studied in our work. We find that 3FGL J1924.8-1034 is the only source which passes the spatial extension test at a confidence level $> 5\sigma$ and 3FGL J2212.5 + 0703 is also spatially extended at a relatively lower confidence level of 4.7σ.

Bertoni *et al.* [35] have analyzed the unidentified, stable and bright (i.e., with the gamma-ray flux $F_\gamma > 7 \times 10^{-10}$ cm^{-2} s^{-1} when integrated above 1 GeV) sources at high galactic latitudes ($|b| > 5°$) and found that 3FGL J2212.5 + 0703 stands out as a subhalo candidate but 3FGL J1924.8-1034 does not. To understand the difference we would like to compare the difference between the data processing procedures. Bertoni *et al.* [35] did not fit the best position of 3FGL J1924.8-1034 by themselves; instead they adopted the position reported in 3FGL that was based on four years of Fermi-LAT data. In this work, the best position fitted with the latest data (deviating from the 3FGL position by ∼0.1 deg) is adopted in the following analysis. The other difference is that we adopt Pass 8 data while just Pass 7 data was available in the previous study.

Since 3FGL J2212.5 + 0703 has already been discussed in great detail in the literature [35,41,43], in the rest of this work we focus on the unidentified gamma-ray source 3FGL J1924.8-1034 and analyze the spatial distribution, light curve and spectrum of the gamma-ray emission from this source. The possibility that the spatial extension of 3FGL J1924.8-1034 is due to the contamination of a nearby unresolved point source is also examined.

III. FERMI DATA ANALYSIS

To study the variability, spectrum and morphology of 3FGL J1924.8-1034, we use 94 months of Pass 8 LAT data from August 27, 2008 (MET = 239500801s) to June 1, 2016 (MET = 486432004s) in the SOURCE event class with the standard conversion-type (FRONT + BACK) selection. Photons with an energy range between 300 MeV and 300 GeV are taken into consideration. 3FGL J1924.8-1034, at a galactic latitude of $b = -12.08°$, is close to the galactic disk, and photons below 300 MeV are contaminated by the diffuse galactic emission. The zenith angle cut $\theta < 90°$ is applied to reduce the contribution from the Earth's limb and we adopt the recommended quality-filter cuts (DATA_QUAL > 0 and LAT_CONFIG == 1) to extract the good time intervals. Then we create $14° \times 14°$ regions of interest (ROIs) centered on (RA, DEC, J2000) = (291.21°, −10.58°) [42] and perform a standard binned likelihood analysis with 0.05° spatial bins and 30 logarithmic energy bins. FERMI SCIENCE TOOLS v10r0p5 and the instrument response functions P8R2_SOURCE_V6 are used for this analysis, which are available from the Fermi Science Support Center.[1]

Utilizing the user-contributed script make3FGLxml.py,[2] we design our model as a combination of the latest model for diffuse Galactic gamma-ray emission (gll_iem_v06.fits), the latest isotropic emission for the SOURCE photon data selection (iso_P8R2_SOURCE_V6_v06.txt) and all 3FGL sources found within a 20° of our ROI. We free the normalizations and spectral indices of all sources within 7° from the target source and the normalizations of the two diffuse emission backgrounds in the maximum likelihood fit. We take the *PowerLaw* as the spectral shape of 3FGL J1924.8-1034, which is the default setting of 3FGL J1924.8-1034 in the 3FGL [42]. To perform the fit and get an optimized model, we use the Fermi-LAT *pyLikelihood* code, utilizing the MINUIT algorithm [44].

We derive a $10° \times 10°$ test statistic (TS) map by placing a test point source at the location of each pixel of the map and maximizing the likelihood which is implemented in the *gttsmap* tool.[3] The TS is defined as TS = $-2\ln(\mathcal{L}_{max,0}/\mathcal{L}_{max,1})$ following Ref. [45], where $\mathcal{L}_{max,0}$ is the maximum likelihood value for a model without an additional source (the null hypothesis) and $\mathcal{L}_{max,1}$ is for a model with that additional source (the alternative hypothesis). We find two new point sources with a TS value larger than 25 and add them to our model with power-law spectra located at the corresponding positions on the TS map. With the help of *gtfindsrc*, we find the optimized positions of the target source 3FGL J1924.8-1034 and two new added sources shown in Table I. The $5° \times 5°$ TS map with (without) a point target source is displayed in Fig. 1.

A. The spatial extension

To determine whether 3FGL J1924.8-1034 exhibits any evidence of spatial extension, we replace the point-source

---

[1]http://fermi.gsfc.nasa.gov/ssc/.
[2]http://fermi.gsfc.nasa.gov/ssc/data/analysis/user/.
[3]http://fermi.gsfc.nasa.gov/ssc/data/analysis/scitools/help/gttsmap.txt.

| Source name	R.A. [°]	Decl. [°]
3FGL J1924.8-1034	291.24	−10.48
newps1	288.20	−12.83
newps2	293.49	−10.41

template with a series of extended templates and vary the width as a free parameter [35,43]. We measure the width by the parameter θ_{68}, defined as the angular radius which contains 68% of the total photons from the target source.

It is difficult to attribute an astrophysical origin to a spatially extended stable source without any association in other wavelengths. Instead it is expected for the massive or nearby dark matter subhalo [41]. The density in the dark matter host halo is often considered as a Navarro-Frenk-White (NFW) profile [46,47]. However, the shapes of nearby subhalos, which are significantly altered by tidal effects, are generally not well described by NFW density profiles. Instead they prefer NFW profiles with an exponential cutoff [48–52] or power-law profiles with an exponential cutoff (PLE) [53].

For completeness, we choose three kinds of distribution for the extension: (1) a two-dimensional Gaussian distribution (GAUSS) [35], (2) a distribution corresponding to a NFW dark matter density profile [41], and (3) a distribution corresponding to a PLE dark matter density profile [53]. The NFW density profile is given by [46,47]

$$\rho(r) = \frac{\rho_0}{(r/R_s)[1 + (r/R_s)]^2} \tag{1}$$
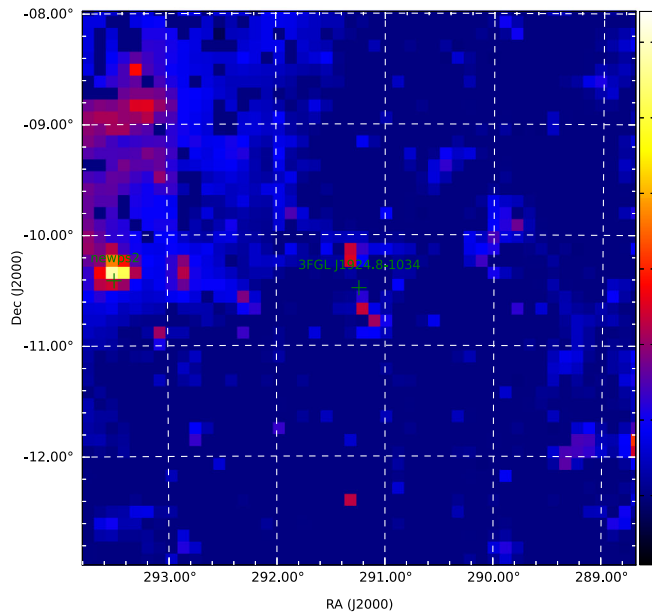
where R_s is the subhalo's scale radius. We adopt the mass-concentration model presented in Ref. [52] for subhalos.

The PLE density profile is given by

$$\rho(r) = \frac{\rho_0}{r^\gamma}\exp\left(-\frac{r}{R_b}\right), \tag{2}$$

where the index γ is taken as 0.74 and R_b is the cutoff radius [53].

The extended template corresponding to the dark matter density $\rho(r)$ [where $r(\theta, d, l) = \sqrt{d^2 + l^2 - 2dl\cos\theta}$] is governed by

$$f(\theta) = \frac{\int_{l=0}^{\infty} \rho^2(r(\theta, d, l))dl}{\int_0^{\theta_{max}} 2\pi\theta \int_{l=0}^{\infty} \rho^2(r(\theta, d, l))dld\theta}, \tag{3}$$

where the first integrals are performed over the line of sight, θ is the angle to the center of the subhalo, θ_{max} is the angular radius encompassing the full extension of the subhalo, and d is the distance to the center of the subhalo. The width (θ_{68}) for this extended template can be defined as $\int_0^{\theta_{68}} 2\pi\theta \times f(\theta)d\theta = 68\%$.

In order to compare these spatial templates, we do the likelihood fit with each template. The TS for spatial extension is defined as the change to the log likelihood, when the point-like template is replaced with that of an extended source:

$$\Delta TS_{ext} = -2(\ln\mathcal{L}_{point} - \ln\mathcal{L}_{ext}) \tag{4}$$

where $\mathcal{L}_{point}$ and $\mathcal{L}_{ext}$ are the best-fit likelihood values for the point-source model and the extended model.
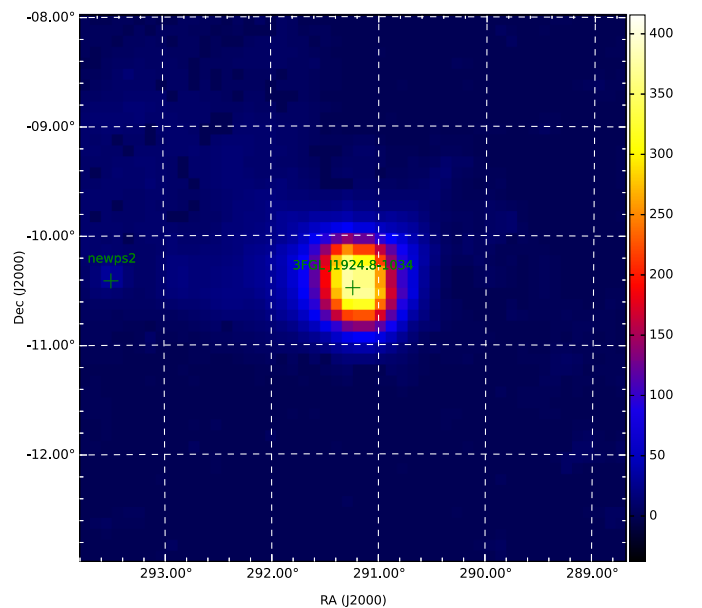

FIG. 1. $5° \times 5°$ TS map centered at the position of 3FGL J1924.8-1034. In the left (right) panel we show the TS map with (without) a point target source included in the modeling. The green crosses represent the positions of the sources within $5° \times 5°$ listed in Table I
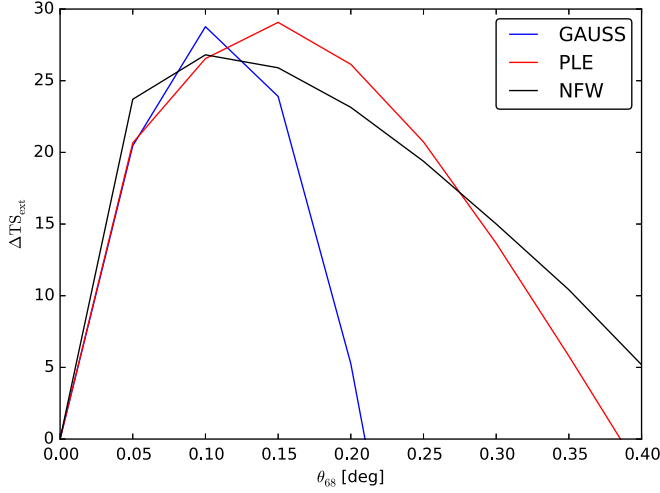
FIG. 2. The ΔTS_{ext} of 3FGL J1924.8-1034 when the point-like template is replaced with a spatial template in the cases of three extension profiles (GAUSS, NFW, PLE). The (GAUSS, NFW, PLE) template fit peaks at $\theta_{68} = (0.1°, 0.1°, 0.15°)$ with a $\Delta TS_{ext} = (28.7, 26.8, 29.1)$, respectively.

The results plotted in Fig. 2, imply that 3FGL J1924.8-1034 prefers a spatially extended profile over that of a single point-like source at a level of $> 5\sigma$ ($\Delta TS_{ext} > 25$) for all three kinds of extended templates and the PLE template with a width of $0.15°$ best describes the data with $\Delta TS_{ext} = 29.1$, corresponding to a statistical significance of 5.4σ. Our results are insensitive on the adopted extension template.

Considering that the Fermi-LAT point spread function (PSF) is large below 3 GeV, we restrict the energy range from 3 to 300 GeV to reselect photons and perform the same analysis. We still find that 3FGL J1924.8-1034 prefers a GAUSS-extended profile with a width of $0.1°$ over that of a single point-like source at a confidence level of 4.2σ ($\Delta TS_{ext} = 17.9$). Moreover we analyze the PSF3-event-type Pass 8 data which has the best angular resolution for a given energy and get $\Delta TS_{ext} = 15.2$ for a $0.1°$-width GAUSS template.

In the above analysis, we choose the spherically symmetric templates to study the spatial extension of 3FGL J1924.8-1034. According to the numerical simulations, whereas isolated dark matter halos tend to be spherical, subhalos are predominantly triaxial [54,55]. So we change the extension template to the spherically symmetric GAUSS template stretched along one axis and free the width, stretch ratio and orientation to repeat the likelihood fit. The stretched template, with a width of $0.1°$, a stretch ratio of 1.3 and a stretched axis oriented approximately $14°$ counterclockwise from the vertical direction, provides the best fit with $\Delta TS_{ext} = 43.8$ corresponding to a statistical significance of 6.0σ for three additional degrees of freedom. The stretched template is preferred over the best-fit spherically symmetric template at a level of $\Delta \ln \mathcal{L} = 14.7$ with two additional degrees of freedom.

However, the Fermi-LAT diffuse model is far from perfect. Some small-size diffuse structures may not be present in this model, which may lead to biased conclusions. Such a possibility cannot be ruled out for the current source.

B. The variability

Considering that 3FGL only used four years of Fermi-LAT data, there is a need to check whether the signal from 3FGL J1924.8-1034 has been stable for almost eight years (see also Ref. [43]). To calculate the light curve of 3FGL J1924.8-1034, we divide these photons into 16 equal time bins. We fix all the parameters except the normalizations of the target source and the diffuse backgrounds in the optimized model. The likelihood fits are performed with this modified model independently in each time bin. The light curve of 3FGL J1924.8-1034 is shown in Fig. 3. To test the variability of 3FGL J1924.8-1034, a variability index is constructed as [43,56],

$$TS_{var} = -2\sum_i \frac{\Delta F_i^2}{\Delta F_i^2 + f^2 F_{const}^2} \ln \frac{\mathcal{L}_i(F_{const})}{\mathcal{L}_i(F_i)}. \quad (5)$$

$\mathcal{L}_i(F_{const})$ is the value of the likelihood in the i-th bin under the null hypothesis where the source flux is constant across the full period and F_{const} is the constant flux for the this hypothesis, while $\mathcal{L}_i(F_i)$ is the value under the alternate hypothesis where the flux in the i-th bin is optimized. For each time bin, the photon flux over the full energy range (300 MeV to 300 GeV) is F_i, and its statistical error is ΔF_i. And we take $f = 2\%$ as the systematic correction factor [42].

If the null hypothesis is correct, TS_{var} is distributed as χ^2 with 15 degrees of freedom [57]. We find $TS_{var} = 13$ and the alternative hypothesis has a low significance of 0.52σ.
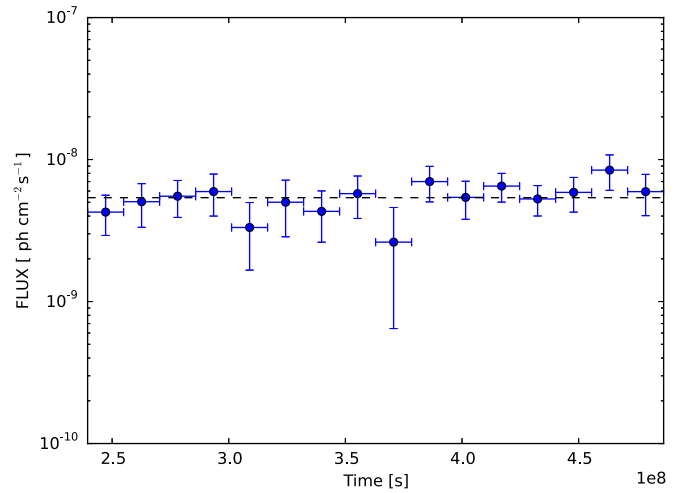

FIG. 3. The light curve of 3FGL J1924.8-1034. The blue point is the photon flux integrated from 300 MeV to 300 GeV in each time bin, and the dashed line is the mean value of all blue points.

So the null hypothesis is reasonable and 3FGL J1924.8-1034 is a nonvariable source.

C. The spectrum

From the above analysis, we identify 3FGL J1924.8-1034 as a stable and spatially extended gamma-ray source without any association in other wavelengths, which makes it a potential candidate for a dark matter subhalo. We assume that the gamma-ray emission observed from 3FGL J1924.8-1034 was generated by DM annihilation. The gamma-ray intensity generated by DM annihilation in the DM subhalo can be described by

$$\Phi(E) = \frac{1}{4\pi} \frac{\langle \sigma v \rangle}{2m_\chi^2} \frac{dN}{dE} \cdot J_{\text{factor}}, \qquad (6)$$

where $\langle \sigma v \rangle$ is the annihilation cross section averaged by the DM velocity and m_χ is the rest mass of the DM particle. J_{factor} is the integration of the square of the DM density $\rho(r)$ along the line of sight s, i.e.,

$$J_{\text{factor}} = \int_\Omega \int_{s=0}^\infty \rho^2(r(s)) \mathrm{d}s \mathrm{d}\Omega. \qquad (7)$$

We change the spectral model to *DMFitFunction*[4] and perform the likelihood fit with this DM model allowing the DM mass (m_χ) and J_{factor} to float freely. In the case of dark matter annihilating into $b\bar{b}$ with the annihilation cross section $\langle \sigma v \rangle = 3 \times 10^{-26}$ cm^3/s [58], the data agrees with a DM mass (m_χ) of 43.5 GeV (see Fig. 4).

To yield the model-independent spectrum of 3FGL J1924.8-1034, we divide the data into 15 evenly spaced logarithmic energy bins from 300 MeV to 300 GeV. We fix the spectral indices of all sources, and leave their normalizations free in the optimized model. The likelihood fit is performed in each energy bin and the resulting spectral energy distribution (SED) plotted in Fig. 4 is similar to that of the Galactic center excess [26–28].

The default setting for the spectral model of 3FGL J1924.8-1034 is *PowerLaw* in the 3FGL [42]. According to the derived SED, we consider some other spectral models (i.e., *LogParabola* and *PLSuperExpCutoff*) to perform the likelihood fit (see Fig. 4). Comparing with the *DMFitFunction* model, we find $\Delta \ln \mathcal{L} = 4.2$ for the *PLSuperExpCutoff* model (only 1.3 for the *LogParabola* model, −27.4 for the default *PowerLaw* model). However the two spectral models are not nested, so the Wilks theorem does not work and a comparison between them is not straightforward [57,59]. Below we adopt the Akaike information criterion (AIC) test [60,61] to check which one is better. The AIC is defined as

___

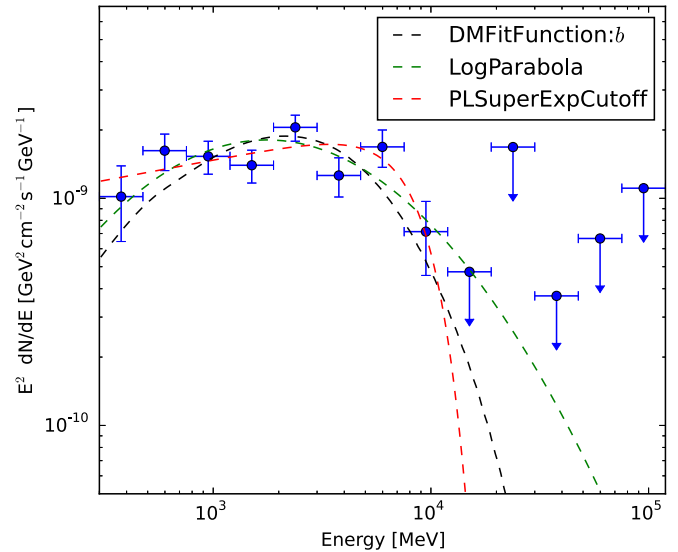[4]http://fermi.gsfc.nasa.gov/ssc/data/analysis/scitools/source_models.html.

FIG. 4.   The spectral energy distribution (SED) of 3FGL J1924.8-1034 (blue). Three types of spectra are shown in this figure, including the *PLSuperExpCutoff* spectrum (red dashed line), the *LogParabola* spectrum (green dashed line) and the *DMFitFunction* spectrum of dark matter annihilation into $b\bar{b}$ (for a rest mass of 43.5 GeV) (black dashed line).

$$\text{AIC} = 2k - 2\ln \mathcal{L} \qquad (8)$$

where k is the number of parameters of the corresponding model and the model that has a smaller AIC is the better one.

The *PLSuperExpCutoff* model has two more spectral parameters than the *DMFitFunction* model and the *PowerLaw* model, and one more spectral parameter than the LogParabola model. So our results $\text{AIC}_{\text{PLSuperExpCutoff}} < \text{AIC}_{\text{DMFitFunction}} < \text{AIC}_{\text{LogParabola}} < \text{AIC}_{\text{PowerLaw}}$ indicate that the *PLSuperExpCutoff* model provides a better spectral fit than other models. Due to the rather small $\Delta \ln \mathcal{L}$, the superiority for the *PLSuperExpCutoff* model is too small to draw a conclusion.

1. Nearby source confusion

Two or more point-like gamma-ray sources in slightly different directions (i.e., the separation between these sources is comparable with or even smaller than the angular resolution of the detector) will be identified as a single spatially extended source. To check such a possibility we define $\Delta \text{TS}_{\text{2pts}}$ as twice the increase in the log of the likelihood of the two close point-like sources model compared to that of the one point-like source model:

$$\Delta \text{TS}_{\text{2pts}} = -2(\ln \mathcal{L}_{\text{point}} - \ln \mathcal{L}_{\text{2pst}}). \qquad (9)$$

Placing a point source A at the catalog position of 3FGL J1924.8-1034 (291.21°, −10.58°), we find the best-fit position (291.29°, −10.32°) of the other source B with the help of *gtfindsrc*. Then we fix the source B position at

(291.29°, −10.32°) and find the best-fit position of the source A (291.21°, −10.61°). The difference between the best-fit position and the original location of source A is only 0.02°, which is well within the LAT PSF. We notice that the angular separation of these overlapping sources is 0.3°. The observed number of sources in 3FGL within 0.3° of another one is less than the expected true number of sources within 0.3° of another one (if sources could be detected at arbitrarily small angular separations) in Fig. 13 of Ref. [42], implying that there could indeed be a nearby source.

To limit the number of new additional degrees of freedom, we just take the *PowerLaw* as the spectral shape of these two point-like sources. Fitting the spectra of the two point-like sources using the best-fit positions, we get $\Delta TS_{2pts} = 58.3$, which is larger than $\Delta TS_{ext} = 43.8$ for the stretched extended template, i.e., we have $\Delta \ln \mathcal{L} = 14.5$ for an additional degree of freedom. However ΔTS_{2pts} cannot be quantitatively compared with ΔTS_{ext} by using the simple likelihood-ratio test because the models are not nested [57,59]. Then we also use the AIC test to evaluate which model is significantly better. Compared to the stretched extended template, the two point-like sources model has one more parameter (two more spatial parameters and two more spectral parameters compared to three more extension parameters). We finally have $AIC_{ext} > AIC_{2pts}$ (note that $\Delta TS_{ext} + 2 < \Delta TS_{2pts}$ and the difference is 12.5), indicating that the data shows a slight preference for the two-point source hypothesis. However, the difference between these two models is small and the dark matter subhalo hypothesis cannot be ruled out.

If 3FGL J1924.8-1034 is actually composed of two point-like sources, one or both of them could have possible counterparts at other wavelengths. So we search for them in four multiwavelength catalogs: (1) the Roma BZCAT— 5th edition Multi-frequency Catalogue of Blazars[5] [62], (2) CRATES—CRATES Flat-Spectrum Radio Source Catalog[6] [63], (3) CGRABS—Candidate Gamma-Ray Blazar Survey Source Catalog[7] [64], and (4) the ATNF Pulsar Catalogue[8] [65]. There are two sources found within 1° of 3FGL J1924.8-1034 (291.21°, −10.58°), including 5BZBJ1925-1018/CRATES J192503-101834 (0.28° away from 3FGL J1924.8-1034) and CRATES J192627-100555 (0.63° away). Further multiwavelength studies are needed to establish or rule out the association of these two sources with the possible source B found in our analysis.

D. The implications

In the following analysis, we assume that 3FGL J1924.8-1034 is a dark matter subhalo to study its properties. From

---

[5]http://www.asdc.asi.it/bzcat/.
[6]https://heasarc.gsfc.nasa.gov/W3Browse/radio-catalog/crates .html.
[7]https://heasarc.gsfc.nasa.gov/W3Browse/radio-catalog/ cgrabs.html.
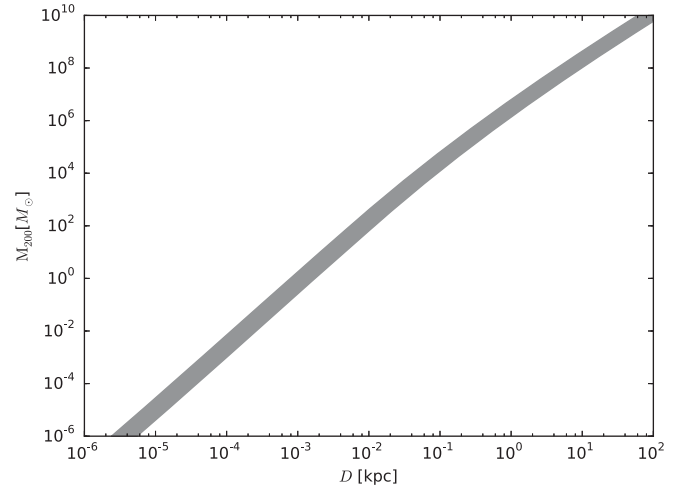[8]http://www.atnf.csiro.au/research/pulsar/psrcat/.

FIG. 5.   The relationship between the subhalo mass (M_{200}) and the distance (D) of the subhalo. The width of the grey band includes the effect of scatter in the subhalo's concentration and mass loss for tidal stripping.

the fit with the DM model ($b\bar{b}$, $\langle \sigma v \rangle = 3 \times 10^{-26}$ cm³/s), we obtain that the gamma-ray flux of the subhalo from 300 MeV to 300 GeV is $(3.59 \pm 0.56) \times 10^{-9}$ ph cm⁻² s⁻¹, with $m_\chi = (43.5 \pm 5.7)$ GeV and $J_{factor} = (3.45 \pm 0.54) \times 10^{20}$ GeV² cm⁻⁵. In Ref. [66], $L = \int_{V_{sub}} \rho^2(r)d^3r = J_{factor}D^2$ was adopted to calculate the subhalo luminosity (D is the distance of the subhalo from the Earth). We can derive that the luminosity-distance ($L - D$) relationship $L = (7.7 \pm 1.2) \times 10^4 \, M_\odot^2 \, pc^{-3}(D/1 \, kpc)^2$, which is close to the median distance calculated from Via Lactea-II results in Fig. 2 of Ref. [66]. So the dark matter subhalo hypothesis seems viable.

The gamma-ray flux of 3FGL J1924.8-1034 can also be used to constrain the mass and distance of the corresponding dark matter subhalo. The concentration model presented in Ref. [52] which was specifically derived for subhalos is adopted in this calculation. In Fig. 5, we plot the relationship between the subhalo mass M_{200} (before tidal stripping) and the distance D of the corresponding subhalo. The grey band reflects the results for scatter in the subhalo's concentration within a factor of 1.7 and a mass loss 90% due to tidal stripping. However just from the flux, it is not possible to draw further conclusions on the subhalo's mass.

IV. SUMMARY AND DISCUSSION

In this work we have analyzed the spatial distribution, variability and spectrum of the gamma-ray emission from the unassociated source 3FGL J1924.8-1034. First, for the spatial extension analysis, we took into account three kinds of dark matter distribution templates. In all cases 3FGL J1924.8-1034 prefers a spatially extended profile over that of a single point-like source (see Fig. 2), and the PLE template with an extension radius of 0.15° best describes

the data at a high confidence level of 5.4σ. Then we compute the light curve of this source and find no significant evidence for deviation from a constant flux. The spectrum of this source is well described by dark matter annihilation into $b\bar{b}$ with a mass of 43.5 GeV, similar to the value required to interpret the Galactic center gamma-ray excess. Therefore we conclude that 3FGL J1924.8−1034 is a stable, spatially extended and unidentified gamma-ray source with a DM-like spectrum.

Dark matter annihilations taking place in some relatively massive and nearby subhalos could appear as stable and spatially extended gamma-ray sources without detectable counterparts in other bands. Hence, 3FGL J1924.8−1034 may be a dark matter subhalo candidate though an astrophysical origin cannot be convincingly ruled out. In particular, the spectrum of 3FGL J1924.8−1034 is also well described by the spectral shape of *PLSuperExpCutoff* which is the spectral model of pulsars. Multiple sources could be misidentified as an extended source. So it is possible that 3FGL J1924.8−1034 is actually made up of two or more gamma-ray sources located close to each other in the sky. Although the LAT data shows preference for the two nearby point-like gamma-ray sources model, the improvement compared to the stretched extended template is small and the dark matter subhalo hypothesis cannot be ruled out. Supposing that 3FGL J1924.8−1034 is indeed from a dark matter subhalo, we have studied the luminosity-distance $(L-d)$ relationship (which agrees with the simulation data; see Sec. II D) and the mass-distance $(M_{200}-d)$ relationship. Further analysis is thus encouraged to confirm or rule out the dark matter subhalo nature of 3FGL J1924.8−1034.

[9]http://fermi.gsfc.nasa.gov/ssc/.

[1] G. Jungman, M. Kamionkowski, and K. Griest, Phys. Rep. **267,** 195 (1996).

[2] G. Bertone, D. Hooper, and J. Silk, Phys. Rep. **405,** 279 (2005).

[3] D. Hooper and S. Profumo, Phys. Rep. **453,** 29 (2007).

[4] J. L. Feng, Annu. Rev. Astron. Astrophys. **48,** 495 (2010).

[5] D. Hooper and S. Profumo, Phys. Rep. **453,** 29 (2007).

[6] E. Charles *et al.*, Phys. Rep. **636,** 1 (2016).

[7] W. Atwood *et al.* (Fermi-LAT Collaboration), Astrophys. J. **697,** 1071 (2009).

[8] M. Ackermann *et al.* (Fermi-LAT Collaboration), Phys. Rev. Lett. **107,** 241302 (2011).

[9] M. Ackermann *et al.* (Fermi-LAT Collaboration), Phys. Rev. D **89,** 042001 (2014).

[10] M. Ackermann *et al.* (Fermi-LAT Collaboration), Phys. Rev. Lett. **115,** 231301 (2015).

[11] D. Hooper and T. Linden, J. Cosmol. Astropart. Phys. 09 (2015) 016.

[12] A. Geringer-Sameth, M. G. Walker, S. M. Koushiappas, S. E. Koposov, V. Belokurov, G. Torrealba, and N. Wyn Evans, Phys. Rev. Lett. **115,** 081101 (2015).

[13] A. Drlica-Wagner *et al.*, Astrophys. J. Lett. **809,** L4 (2015).

[14] A. Geringer-Sameth, S. M. Koushiappas, and M. G. Walker, Phys. Rev. D **91,** 083535 (2015).

[15] S. Li, Y.-F. Liang, K.-K. Duan, Z.-Q. Shen, X. Huang, X. Li, Y.-Z. Fan, N.-H. Liao, L. Feng, and J. Chang, Phys. Rev. D **93,** 043518 (2016).

[16] A. Albert *et al.* (Fermi-LAT and DES Collaborations), Astrophys. J. **834,** 110 (2017).

[17] X. Huang, G. Vertongen, and C. Weniger, J. Cosmol. Astropart. Phys. 01 (2012) 042.

[18] Q. Yuan, P.-F. Yin, X.-J. Bi, X.-M. Zhang, and S.-H. Zhu, Phys. Rev. D **82,** 023506 (2010).

[19] S. Ando and D. Nagai, J. Cosmol. Astropart. Phys. 07 (2012) 017.

[20] M. Ackermann *et al.* (Fermi-LAT Collaboration), Astrophys. J. **812,** 159 (2015).

[21] Y. F. Liang, Z.-Q. Xia, Z.-Q. Shen, X. Li, W. Jiang, Q. Yuan, Y.-Z. Fan, L. Feng, E.-W. Liang, and J. Chang, Phys. Rev. D **94,** 103502 (2016).

[22] M. Ajello *et al.* Astrophys. J. **819,** 44 (2016).

[23] D. Hooper and L. Goodenough, Phys. Lett. B **697,** 412 (2011).

[24] C. Gordon and O. Macías, Phys. Rev. D **88,** 083521 (2013).

[25] D. Hooper and T. R. Slatyer, Phys. Dark Univ. **2,** 118 (2013).

[26] B. Zhou, Y.-F. Liang, X. Huang, X. Li, Y.-Z. Fan, L. Feng, and J. Chang, Phys. Rev. D **91,** 123010 (2015).

[27] F. Calore, I. Cholis, and C. Weniger, J. Cosmol. Astropart. Phys. 03 (2015) 038.

[28] X. Y. Huang, T. Enßlin, and M. Selig, J. Cosmol. Astropart. Phys. 04 (2016) 030.

[29] M. Ackermann *et al.* (Fermi-LAT collaboration), J. Cosmol. Astropart. Phys. 09 (2015) 008.

[30] M. Di Mauro and F. Donato, Phys. Rev. D **91,** 123001 (2015).

[31] W. Liu, X.-J. Bi, S.-J. Lin, and P.-F. Yin, Chin. Phys. C **41,** 045104 (2017).

[32] S. D. White and C. S. Frenk, Astrophys. J. **379,** 52 (1991).

[33] V. Springel, J. Wang, M. Vogelsberger, A. Ludlow, A. Jenkins, A. Helmi, J. F. Navarro, C. S. Frenk, and S. D. M. White, Mon. Not. R. Astron. Soc. **391,** 1685 (2008).

[34] M. Kuhlen, P. Madau, and J. Silk, Science **325,** 970 (2009).

[35] B. Bertoni, D. Hooper, and T. Linden, J. Cosmol. Astropart. Phys. 12 (2015) 035.

[36] M. Kuhlen, J. Diemand, and P. Madau, Astrophys. J. **686,** 262 (2008).

[37] B. Anderson, M. Kuhlen, J. Diemand, R. P. Johnson, and P. Madau, Astrophys. J. **718,** 899 (2010).

[38] M. R. Buckley and D. Hooper, Phys. Rev. D **82,** 063501 (2010).

[39] D. Schoonenberg, J. Gaskins, G. Bertone, and J. Diemand, J. Cosmol. Astropart. Phys. 05 (2016) 028.

[40] Q. Yuan, Y. Cao, J. Liu, P.-F. Yin, L. Gao, X.-J. Bi, and X. Zhang, Phys. Rev. D **86,** 103531 (2012).

[41] B. Bertoni, D. Hooper, and T. Linden, J. Cosmol. Astropart. Phys. 05 (2016) 049.

[42] F. Acero *et al.* (Fermi-LAT Collaboration), Astrophys. J. Suppl. Ser. **218,** 23 (2015).

[43] Y. P. Wang *et al.*, Phys. Rev. D **94,** 123002 (2016).

[44] F. James and M. Roos, Comput. Phys. Commun. **10,** 343 (1975).

[45] J. R. Mattox *et al.*, Astrophys. J. **461,** 396 (1996).

[46] J. F. Navarro, C. S. Frenk, and S. D. White, Astrophys. J. **462,** 563 (1996).

[47] J. F. Navarro, C. S. Frenk, and S. D. White, Astrophys. J. **490,** 493 (1997).

[48] S. Ghigna, B. Moore, F. Governato, G. Lake, T. Quinn, and J. Stadel Mon. Not. R. Astron. Soc. **300,** 146 (1998).

[49] S. Kazantzidis, A. V. Kravtsov, A. R. Zentner, B. Allgood, D. Nagai, and B. Moore Astrophys. J. **611,** L73 (2004).

[50] J. Diemand, M. Kuhlen, and P. Madau, Astrophys. J. **657,** 262 (2007).

[51] J. Diemand, M. Kuhlen, and P. Madau, Astrophys. J. **667,** 859 (2007).

[52] Á. Moliné *et al.* Mon. Not. R. Astron. Soc. **466,** 4974 (2017).

[53] D. Hooper and S. J. Witte, arXiv:1610.07587.

[54] M. Kuhlen, J. Diemand, and P. Madau, Astrophys. J. **671,** 1135 (2007).

[55] C. A. Vera-Ciro, L. V. Sales, A. Helmi, and J. F. Navarro Mon. Not. R. Astron. Soc. **439,** 2863 (2014).

[56] P. L. Nolan *et al.* (Fermi-LAT Collaboration), Astrophys. J. Suppl. Ser. **199,** 31 (2012).

[57] S. S. Wilks, Ann. Math. Stat. **9,** 60 (1938).

[58] G. Steigman, B. Dasgupta, and J. F. Beacom, Phys. Rev. D **86,** 023506 (2012).

[59] S. Algeri, J. Conrad, and D. A. van Dyk, Mon. Not. R. Astron. Soc. **458,** L84 (2016).

[60] J. Lande *et al.*, Astrophys. J. **756,** 5 (2012).

[61] H. Akaike, IEEE Trans. Autom. Control **19,** 716 (1974).

[62] E. Massaro, A. Maselli, C. Leto, P. Marchegiani, M. Perri, P. Giommi, and S. Piranomonte Astrophys. Space Sci. **357,** 75 (2015).

[63] S. E. Healey, R. W. Romani, G. B. Taylor, E. M. Sadler, R. Ricci, T. Murphy, J. S. Ulvestad, and J. N. Winn, Astrophys. J. Suppl. Ser. **171,** 61 (2007).

[64] S. E. Healey, R. W. Romani, G. Cotter, P. F. Michelson, E. F. Schlafly, A. C. S. Readhead, P. Giommi, S. Chaty, I. A. Grenier, and L. C. Weintraub, Astrophys. J. Suppl. Ser. **175,** 97 (2008).

[65] R. N. Manchester, G. B. Hobbs, A. Teoh, and M. Hobbs, Astron. J. **129,** 1993 (2005).

[66] P. Brun, T. Delahaye, J. Diemand, S. Profumo, and P. Salati, Phys. Rev. D **80,** 035023 (2009).